

Datumless Topography: A Universally Consistent Way to Quantify Relief

Kai Xu

Yale University

Abstract

Despite having long been the standard for quantifying relief on Earth and beyond, elevation has its limitations. The zero-elevation datum is defined by arbitrary and inconsistent conventions, especially on planets without a sea level, hence the lack of a universally standardized way to quantify relief. Furthermore, when quantifying relief on such planets, the elevation of a point is rather meaningless on its own, deriving most of its value when compared to the elevation of other points. In light of these considerations, this paper introduces a universally consistent framework for quantifying relief that does not require a datum altogether, and is instead based on physically meaningful concepts. Designed to be mathematically elegant and free of arbitrary parameters, the so-called datumless measures are divided into the datumless point measures and the datumless surface measures. As opposed to elevation, which describes the vertical position of a point relative to a datum, the datumless point measures directly describe the vertical position of a point relative to local terrain, making them useful for comparing the relief of features such as mountains across different planets. In the meantime, the datumless surface measures quantify various aspects of relief within a region, as opposed to that of a single point. This is done through datumless formulations of surface area and surface mean value, which can be directly applied to the fractal-like planetary surface without projecting it onto a reference ellipsoid. Altogether, this paper lays the groundwork for a datumless framework that enables future topographic tasks to transcend the limitations of elevation.

1 Introduction

Central to the field of topography is elevation, which is widely used to quantify relief on Earth and other planets.¹ Yet, despite its ubiquity, elevation has its limitations. The vertical datum, from which elevation is measured, is defined by arbitrary and inconsistent conventions that are subject to change [1]. On Earth, this results in minor elevation differences between differing datums. The greater problem arises on planets without a sea level, where the datum

¹For conciseness, a *planet* will refer to any astronomical object with a terrestrial surface, including moons and asteroids.

is defined especially arbitrarily due to the lack of an obvious terrain feature to base it on, hence the lack of a universally standardized way to quantify relief [2]. Furthermore, when quantifying relief on such planets, the elevation of a point is rather meaningless on its own, deriving most of its value when compared to the elevation of other points. Hence, elevation is better described as a reference frame for comparing height differences, rather than as an absolute measure of relief in and of itself. That is not to disregard elevation altogether, as it is invaluable for many tasks such as mapping, geolocation, and climatology. However, when it comes to the distinct task of quantifying topographic relief, it is beneficial to think outside the datum.

In light of these factors, this paper introduces a universally consistent framework for quantifying relief that does not rely on a datum. The so-called datumless measures are defined purely based on physically meaningful concepts without relying on arbitrary parameters. Designed to be mathematically elegant and easy to understand, the datumless measures can be divided into the datumless point measures and the datumless surface measures.

Following this introduction, the paper first introduces the preliminaries that are required for understanding the datumless measures. Preliminaries include a formal definition of the planetary surface and a way of quantifying the spatial relationship between two points on the planetary surface.

Next up are the datumless point measures, which describe various aspects about the vertical position of a point relative to local terrain (unlike elevation, which describes vertical position relative to an imaginary datum). Perhaps the most widely applicable point measure is *dominance*, which measures how much a point rises above its large-scale surroundings. Among its applications, dominance provides a universally standardized base-to-peak measure of the height of any mountain on any planet. Another practical point measure is *jut*, which measures how sharply a point rises above its immediate surroundings, usually from the bottom of a neighboring valley. Inspired by the omnidirectional relief and steepness (ORS) measure [3], which quantifies the visual impressiveness of a protruding landform, jut achieves this same objective in a way that is more straightforward and easier to visualize geometrically. Several other point measures are also introduced in this section, including the *composite point measures*, which combine different point measures to describe even more aspects of relief.

Following the datumless point measures are the datumless surface measures, which describe the overall relief within a region, as opposed to that of a single point. This section first introduces datumless formulations of surface area and surface mean value that can be directly applied to the fractal-like planetary surface without having to project it onto an arbitrary reference ellipsoid. Then, it uses these definitions to average the datumless point measures over a region, achieving measures of ruggedness, steepness, skewness, and kurtosis. The datumless surface measures are inspired by the surface roughness parameters [4] in mechanical engineering.

The final technical section of this paper describes the process of computing the datumless point measures. This section also displays the values of the point measures at various locations on Earth, Moon, Mars, and Vesta.

2 Preliminaries

2.1 Datumless Definition of the Planetary Surface

This subsection introduces a definition of the planetary surface that does not rely on a reference ellipsoid, and is based instead on meaningful concepts in physics. The provided definition is conducive to both computational representation and mathematical abstraction.

2.1.1 Planet as a Manifold-With-Boundary

Let the universe be represented by 3-dimensional space, or \mathbb{R}^3 . Every location relative to the planet of interest can be mapped to a point² in \mathbb{R}^3 . This paper uses an Earth-Fixed, Earth-Centered (ECEF) coordinate system. Nevertheless, what matters is not the absolute coordinate system, but the relative positions of points with respect to each other.

Let the planet of interest be represented by M , a theoretically infinite set of points in \mathbb{R}^3 , i.e., $M \subset \mathbb{R}^3$. A point in \mathbb{R}^3 is in M if and only if its location is occupied by physical matter that the planet of interest is composed of. Depending on the intentions of measurement, M can be defined to include or exclude matter corresponding to features such as buildings, vegetation, water bodies, and permanent ice and snow.

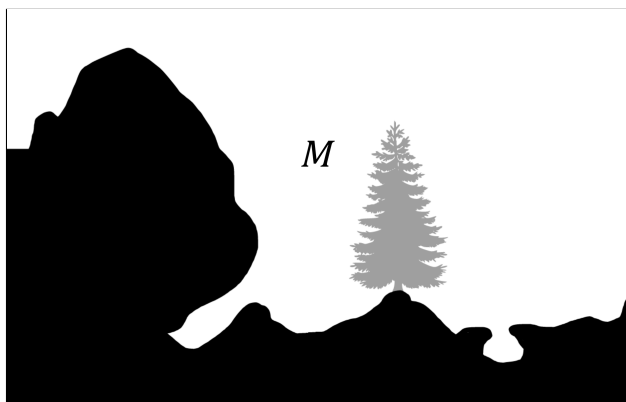


Figure 1: Points in M are shaded in black. Vegetation is excluded in this particular definition of M .

Effectively, M is a manifold-with-boundary—more specifically, a 3-manifold with a 2-dimensional boundary. The boundary of M , denoted by ∂M , comprises of all points in M that are infinitesimally close to a point in \mathbb{R}^3 that is not in M . The boundary can be thought of as the parts of a planet that are directly exposed to the atmosphere (or outer space, if an atmosphere does not exist).

$$\partial M = \{\mathbf{p} \in M \mid (\exists \mathbf{q} \in \{\mathbb{R}^3 \setminus M\} : |\mathbf{p} - \mathbf{q}| = \varepsilon)\}$$

where ε denotes an infinitesimally small quantity.

²The term *point* will refer to a position vector, which provides more notational flexibility than an ordered triple.

∂M has a fractal-like texture all the way down to the microscopic level. It is not useful for topographic applications, as it contains points on cave walls and underneath overhangs, which are not captured by most surface models such as digital elevation models (DEMs). One need not worry about representing M or ∂M digitally—they are merely conceptual intermediaries used to provide a formalized definition of the planetary surface.

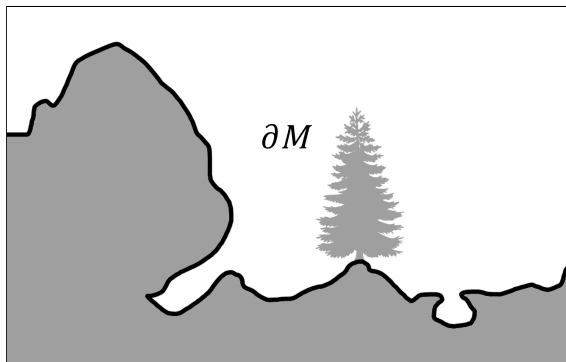


Figure 2: Points in ∂M are outlined in black.

2.1.2 Planetary Surface

A planet’s gravitational field can be depicted as surfaces of constant gravitational potential surrounding the planet—also known as *equipotential surfaces*—to which the direction of gravity is always perpendicular to. *Plumblines* can be defined as curves running perpendicular to the equipotential surfaces, which are therefore tangent to the direction of gravity along their lengths. Roughly speaking, a falling object will travel along its plumbline.

To introduce terminology used in defining the planetary surface, point \mathbf{q} *overhangs* point \mathbf{p} if and only if \mathbf{q} has a higher gravitational potential than \mathbf{p} and also lies on the same plumbline as \mathbf{p} .

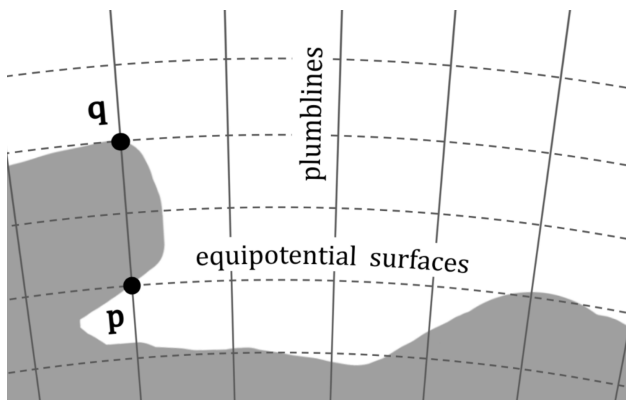


Figure 3: Point \mathbf{q} overhangs point \mathbf{p} in this diagram.

The *planetary surface*, denoted by S , is the subset of ∂M consisting of all points in ∂M that are not overhung by another point in M . The planetary surface can be thought of as

the parts of a planet that are directly exposed to falling raindrops.

$$S = \{\mathbf{p} \in \partial M \mid (\nexists \mathbf{q} \in M \mid \mathbf{q} \text{ overhangs } \mathbf{p})\}$$

S is an infinite set of points, meant to represent a perfect topographic model of infinite resolution. In practice, S can be represented by a surface model such as a DEM,³ converted to a 3-dimensional coordinate system such as ECEF. On Earth, depending on how M is defined and which surface model is used, the planetary surface can either be *wet*, including water surfaces in its set of points, or *dry*, including underwater bathymetry instead. In this paper, S and all derived measurements should be assumed as wet unless stated otherwise.

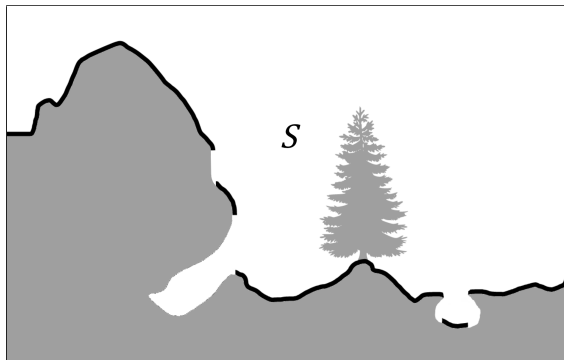


Figure 4: Points in S are outlined in black.

2.2 A Point in the Reference Frame of Another Point

The concepts in this subsection are best understood through the metaphor of point \mathbf{p} being observed from point \mathbf{q} , ignoring viewshed obstructions. For instance, \mathbf{p} could be the summit of a mountain, and \mathbf{q} could be the location of an observer at the bottom of the mountain.

2.2.1 Vertical Unit Vector and Horizontal Plane

Let the *vertical unit vector* of \mathbf{q} , denoted by $\hat{\mathbf{k}}_{\mathbf{q}}$, be the vector of magnitude 1 that points *opposite* the direction of gravity at \mathbf{q} . The vertical unit vector represents the upwards direction of an observer at \mathbf{q} .

Let the *horizontal plane* of \mathbf{q} be the flat plane that $\hat{\mathbf{k}}_{\mathbf{q}}$ is perpendicular to that passes through \mathbf{q} . Another point \mathbf{p} is *above* the horizontal plane of \mathbf{q} if it is on the same side of the plane as $\hat{\mathbf{k}}_{\mathbf{q}}$ points towards, *below* the horizontal plane if it is on the opposite side, and *on* the horizontal plane if it touches it. The horizontal plane represents the “ground level” of an observer at \mathbf{q} .

³The usage of a DEM in this paper is non-arbitrary, as it is for determining the objective position of points on the planetary surface, rather than as a subjective measure of relief.

2.2.2 Height Above the Horizontal Plane

Let the *position vector* of \mathbf{p} with respect to \mathbf{q} , denoted by $\mathbf{r}_{\mathbf{p}\leftarrow\mathbf{q}}$, be the vector pointing from \mathbf{q} to \mathbf{p} , i.e., the difference between their coordinates:

$$\mathbf{r}_{\mathbf{p}\leftarrow\mathbf{q}} = \mathbf{p} - \mathbf{q}$$

The arrow subscript notation as used above denotes an attribute of \mathbf{p} in the reference frame of \mathbf{q} . This notation will continue to be used.

The *height* of \mathbf{p} above the horizontal plane of \mathbf{q} , denoted by $z_{\mathbf{p}\leftarrow\mathbf{q}}$, is equal to the scalar projection of $\mathbf{r}_{\mathbf{p}\leftarrow\mathbf{q}}$ onto the vertical unit vector of \mathbf{q} .

$$z_{\mathbf{p}\leftarrow\mathbf{q}} = \mathbf{r}_{\mathbf{p}\leftarrow\mathbf{q}} \cdot \hat{\mathbf{k}}_{\mathbf{q}}$$

Point \mathbf{p} is above the horizontal plane of \mathbf{q} if $z_{\mathbf{p}\leftarrow\mathbf{q}}$ is positive, on the horizontal plane if $z_{\mathbf{p}\leftarrow\mathbf{q}}$ is 0, and below the horizontal plane if $z_{\mathbf{p}\leftarrow\mathbf{q}}$ is negative. Due to planetary curvature, the height of one point above the horizontal plane of another is not equal to the elevation difference between the two points. For instance, even though Mt. Everest has a much higher elevation than the Dead Sea, Mt. Everest is over 1000 kilometers below the horizontal plane of the Dead Sea.

2.2.3 Angle of Elevation

The *angle of elevation* of \mathbf{p} above the horizontal plane of \mathbf{q} , denoted by $\theta_{\mathbf{p}\leftarrow\mathbf{q}}$, is the signed angle between $\mathbf{r}_{\mathbf{p}\leftarrow\mathbf{q}}$ and the horizontal plane of \mathbf{q} . It is positive if \mathbf{p} is above the horizontal plane of \mathbf{q} , negative if \mathbf{p} is below the horizontal plane, and 0 if \mathbf{p} is on the horizontal plane.

$$\theta_{\mathbf{p}\leftarrow\mathbf{q}} = \arcsin\left(\hat{\mathbf{r}}_{\mathbf{p}\leftarrow\mathbf{q}} \cdot \hat{\mathbf{k}}_{\mathbf{q}}\right)$$

where $\hat{\mathbf{r}}_{\mathbf{p}\leftarrow\mathbf{q}}$ is the position unit vector, defined as follows:

$$\hat{\mathbf{r}}_{\mathbf{p}\leftarrow\mathbf{q}} = \frac{\mathbf{r}_{\mathbf{p}\leftarrow\mathbf{q}}}{|\mathbf{r}_{\mathbf{p}\leftarrow\mathbf{q}}|}$$

The value of $\theta_{\mathbf{p}\leftarrow\mathbf{q}}$ is undefined if $\mathbf{p} = \mathbf{q}$.

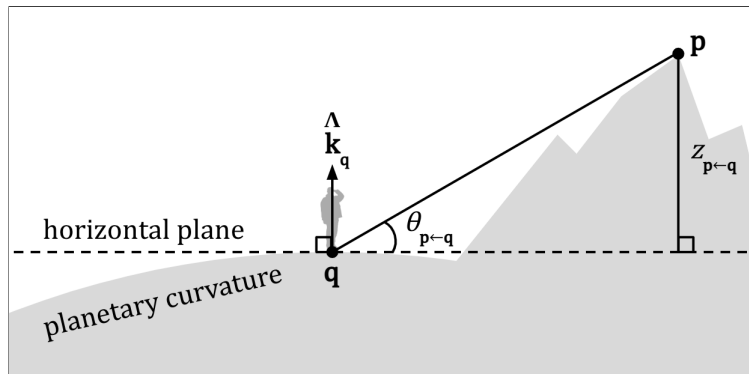


Figure 5: Point \mathbf{p} in the reference frame of point \mathbf{q} .

2.2.4 Angle-Reduced Height

Let the *angle-reduced height* of \mathbf{p} with respect to \mathbf{q} , denoted by $z'_{\mathbf{p}\leftarrow\mathbf{q}}$, be equal to the following:

$$z'_{\mathbf{p}\leftarrow\mathbf{q}} = z_{\mathbf{p}\leftarrow\mathbf{q}} |\sin \theta_{\mathbf{p}\leftarrow\mathbf{q}}|$$

and if $\mathbf{p} = \mathbf{q}$, let $z'_{\mathbf{p}\leftarrow\mathbf{q}} = 0$.

The magnitude of angle-reduced height describes how sharply point \mathbf{p} gains its relief with respect to \mathbf{q} . Its magnitude increases with both a greater height difference and a steeper angle of elevation. Meanwhile, the sign of angle-reduced height describes which side of the horizontal plane of \mathbf{q} that \mathbf{p} is on.

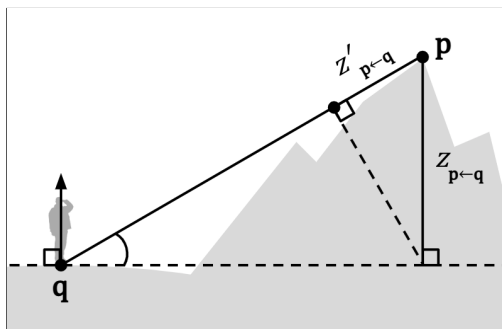


Figure 6: Geometric diagram of angle-reduced height.

Subjectively, angle-reduced height describes how visually impressive point \mathbf{p} appears to an observer at \mathbf{q} . For instance, the impressiveness of a mountain is a result of not only how high it rises, but also the angle at which it does, hence why mountains tend to appear more impressive from close-up. To capture this phenomenon, angle-reduced height is equal to height above the horizontal plane when $\theta_{\mathbf{p}\leftarrow\mathbf{q}}$ is 90° or -90° (akin to a vertical cliff). However, the less steep the angle of elevation, the lower the value of $|\sin(\theta_{\mathbf{p}\leftarrow\mathbf{q}})|$ is and the more the expression for $z'_{\mathbf{p}\leftarrow\mathbf{q}}$ gets reduced.

Earl and Metzler [3] was the first to present a formula that specifically captures the visual impressiveness of a point as observed from another, serving as an inspiration for this paper. In their paper, the formula $H \frac{\theta}{90^\circ}$ was used, where H is the absolute value of the elevation difference between two points and θ is the angle of elevation on a flat Earth model, where the elevation difference and geodetic distance between two points are treated as the legs of a right triangle. Angle-reduced height presents an improvement upon this formula, as it is easier to visualize geometrically, defined for angles greater than 90° , and does not require a datum.

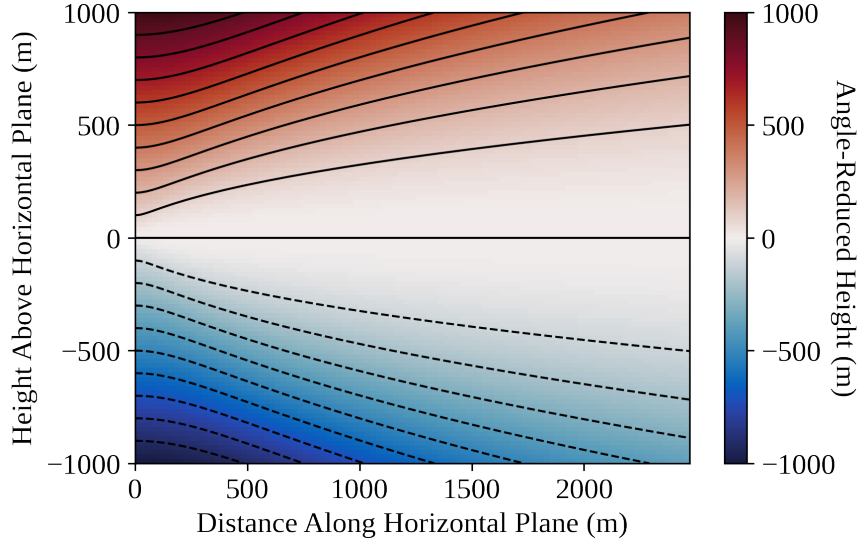


Figure 7: Contour plot of angle-reduced height. If the origin of this graph represents the location of an observer and the horizontal axis represents their horizontal plane, points on the same contour line (and those of the same color) are considered equally impressive to the observer. This graph is created in Matplotlib [5]. The red-white-blue colormap used in this and subsequent visualizations is adapted from cmocean colormaps [6].

3 Datumless Point Measures

The datumless point measures describe various aspects about the relief of a point relative to its surroundings.

3.1 Dominance

The *dominance* of point \mathbf{p} is the maximum height of \mathbf{p} above the horizontal plane of any point on the planetary surface:

$$\text{dom}(\mathbf{p}) = \max_{\mathbf{q} \in S} z_{\mathbf{p} \leftarrow \mathbf{q}}$$

Dominance measures how much a point rises above its surroundings. It is guaranteed to be greater than equal to 0 for any point on the planetary surface (unlike elevation, which may be negative). This is because the height of \mathbf{p} above the horizontal plane of itself is 0, and dominance involves taking a maximum with respect to all surface points, including \mathbf{p} itself. In addition, due to planetary curvature, \mathbf{p} has a negative height with respect to points very far away. Hence, only points within a local vicinity of \mathbf{p} , known as its *curvature-scale surroundings*, are relevant to the calculation of dominance.

The *base* of point \mathbf{p} is the point on the planetary surface with the maximum height of \mathbf{p} above its horizontal plane. The height of \mathbf{p} above the horizontal plane of its base is in turn equal to the dominance of \mathbf{p} . For a point within a mountain range, its base is typically located where the mountain range meets lower plains. The dominance of the summit of

a mountain provides a non-arbitrary base-to-peak measure of the mountain's height. This works for mountains on any terrestrial planet.

On Earth, most points have a base close to sea level, therefore measuring a dominance that is usually only slightly lower than elevation. However, for points with an elevated base, usually on a high plain or plateau, dominance can be significantly lower than elevation, providing a more perceptually accurate measure of height. Consider the summit of Pikes Peak in the Front Range of Colorado. The elevation of the summit is 4352 m, a value that correlates well with the air pressure, climate, and vegetation of the peak. In contrast, its dominance is 2575 m, which captures how much it rises above the neighboring Great Plains. Likewise, a point on the Great Plains may have an elevation above 1000 m, but its dominance will be close to 0, reflecting the sheer flatness of the surroundings.

Dominance is considered a *converging measure* because the arrow in the subscript of the maximized expression points towards \mathbf{p} , the point of interest. Metaphorically, this is akin to looking towards \mathbf{p} from points on the planetary surface, the lines of sight converging at \mathbf{p} . The *converging height map* of \mathbf{p} shows the height of \mathbf{p} above the horizontal planes of points in its surroundings:

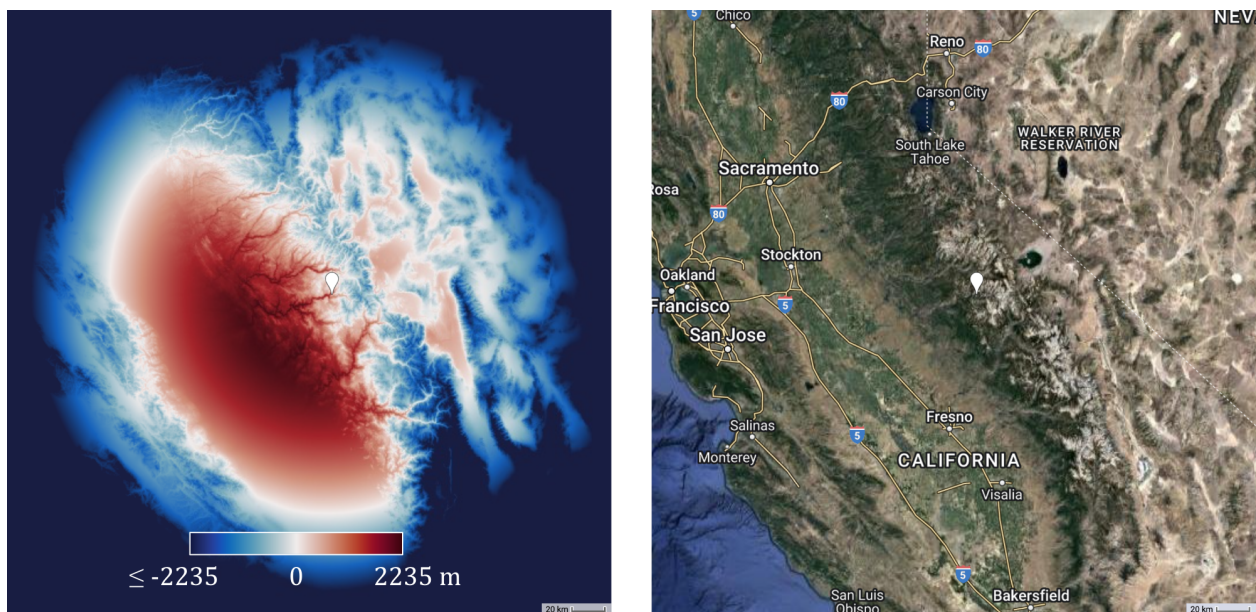


Figure 8: On the left is the converging height map of the summit of Half Dome (displayed as pin), to be overlaid on the base map to the right. The dominance of the summit is the maximum value, 2235 m, measured from its base at the bottom of the Sierra Nevada mountain range where it meets the Central Valley. Values are negative far away due to planetary curvature. Maps are generated in Google Earth Engine [7].

A point with a dominance of 0 is known as a *submissive point*. A submissive point does not rise above the horizontal plane of any point on the planetary surface. Such points are usually found in recessed features such as valleys, canyons, trenches, and craters. An example of a submissive point is Badwater Basin in Death Valley.

3.2 Submission

The *submission* of point \mathbf{p} is the maximum height of any point on the planetary surface above the horizontal plane of \mathbf{p} :

$$\text{sub}(\mathbf{p}) = \max_{\mathbf{q} \in S} z_{\mathbf{q} \leftarrow \mathbf{p}}$$

Submission measures how much a point dips below its surroundings, yielding a value greater than or equal to 0 for any point on the planetary surface. Like dominance, submission can be described as a measure of curvature-scale relief, as points very far away from \mathbf{p} correspond to negative height values that are irrelevant to the calculation of submission.

The point on the planetary surface with the maximum height above the horizontal plane of \mathbf{p} is known as the *roof* of \mathbf{p} . For a point within a mountain range, its roof is usually located at the top of a high mountain within the mountain range.⁴

Submission is a *diverging measure* because the arrow in the subscript of the maximized expression points away from \mathbf{p} . Metaphorically, this is akin to an observer standing at \mathbf{p} and looking away to other points on the planetary surface, the lines of sight diverging from \mathbf{p} . The *diverging height map* of \mathbf{p} shows the height of points in the surroundings of \mathbf{p} above the horizontal plane of \mathbf{p} :

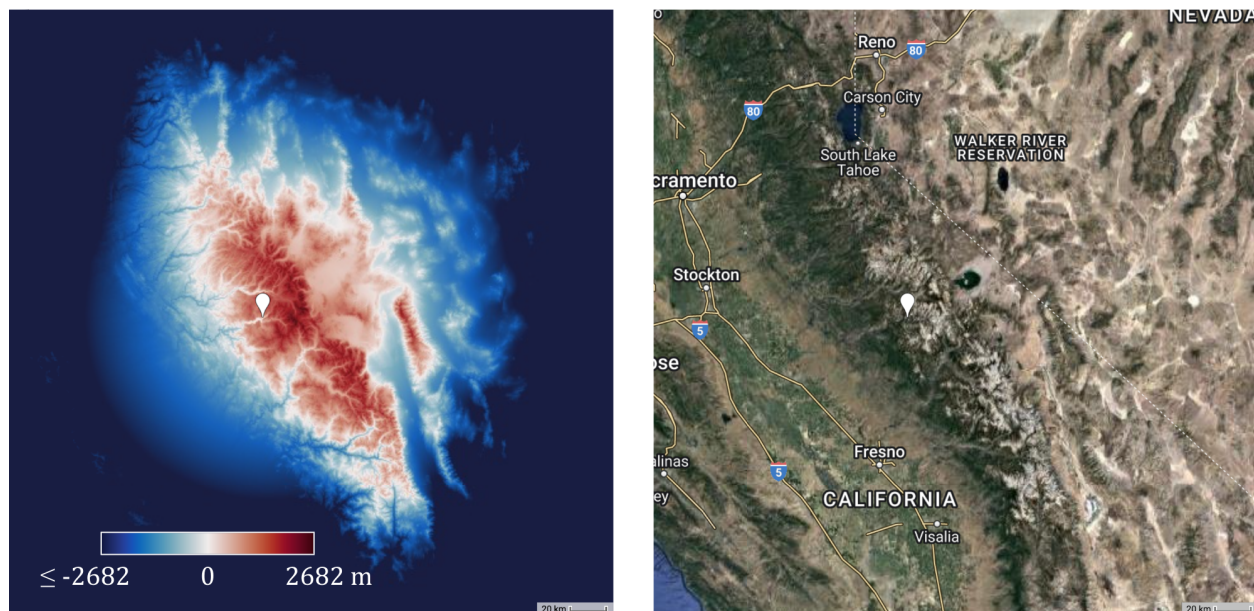


Figure 9: Diverging height map of Mirror Lake in Yosemite Valley. The submission of Mirror Lake is the maximum value, 2682 m, measured at its roof at the top of Mt. Lyell, the highest mountain in Yosemite National Park. Values are negative far away due to planetary curvature.

A point with a submission of 0 is known as a *dominant point*. A person standing at a dominant point is “on top of the world,” as no point rises above their horizontal plane.

⁴It may be interesting to note that base of the point with the greatest dominance on a planet (Mt. Everest on Earth) is the point with the greatest submission, and the roof of the point with the greatest submission on a planet is the point with the greatest dominance.

Dominant points are usually found on protruding features such as mountains, hills, and islands. An example of a dominant point is the summit of Mt. Whitney, the highest point of the Sierra Nevada in terms of both dominance and elevation.

3.3 Jut

The *jut* of point \mathbf{p} is the maximum angle-reduced height of \mathbf{p} with respect to any point on the planetary surface:

$$\text{jut}(\mathbf{p}) = \max_{\mathbf{q} \in S} z'_{\mathbf{p} \leftarrow \mathbf{q}}$$

Jut measures how sharply a point rises above its immediate surroundings, yielding a greater value for higher and steeper rises. It is greater than or equal to 0 for any point on the planetary surface. Jut is inspired by the omnidirectional relief and steepness (ORS) measure [3], which was designed to capture the visual impressiveness of a mountain peak or other protruding feature. Jut achieves the same objective in a much simpler way, as it only requires taking a maximum, as opposed to a surface integral in the case of ORS.

The point on the planetary surface that measures the maximum angle-reduced height of \mathbf{p} with respect to itself is known as the *immediate base* of \mathbf{p} . For a point within a mountain range, its immediate base is usually at the bottom of a neighboring valley (as opposed to its base, which is usually at the bottom of a mountain range).

Jut is a converging measure because the arrow in the subscript of the maximized expression points towards \mathbf{p} . The *converging angle-reduced height map* of point \mathbf{p} shows the angle-reduced height of \mathbf{p} with respect to points in its surroundings:

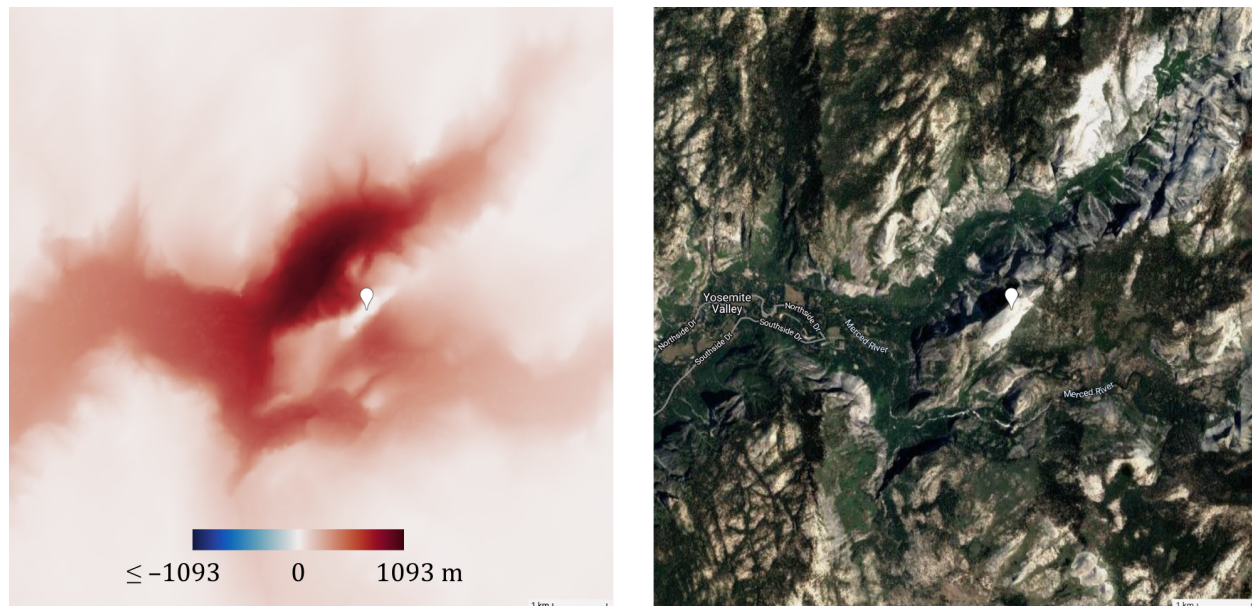


Figure 10: Converging angle-reduced height map of the summit of Half Dome. The jut of the summit is the maximum value, 1093 m, measured from its immediate base in Yosemite Valley near Mirror Lake.

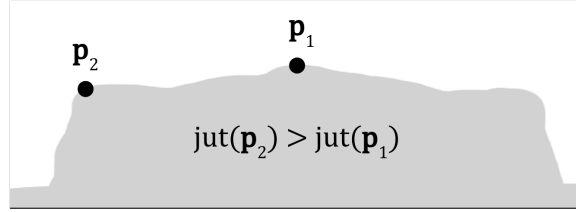


Figure 11: The point on a mountain with the highest jut is not necessarily its peak. A real-world example is El Capitan in Yosemite, whose maximum jut is measured near the edge of its cliff rather than at higher locations further away from the cliff.

3.4 Rut

The *rut* of point \mathbf{p} is the maximum angle-reduced height of any point on the planetary surface with respect to \mathbf{p} :

$$\text{rut}(\mathbf{p}) = \max_{\mathbf{q} \in S} z'_{\mathbf{q} \leftarrow \mathbf{p}}$$

Rut measures how sharply or impressively a point dips below its immediate surroundings, accounting for both height differences and steepness. It is greater than or equal to 0 for any point on the planetary surface.

The point on the planetary surface with the maximum angle-reduced height with respect to \mathbf{p} is known as the *immediate roof* of \mathbf{p} . For a point within a mountain range, its immediate roof is usually at the top of a neighboring mountain (as opposed to its roof, which is usually at the top of a superlative mountain in the mountain range).⁵

Rut is a converging measure because the arrow in the subscript of the maximized expression points away from \mathbf{p} . The *diverging angle-reduced height map* of point \mathbf{p} shows the angle-reduced height of points in the surroundings of \mathbf{p} with respect to \mathbf{p} :

⁵It may be interesting to note that the immediate base of the point with the greatest jut on a planet is the point with the greatest rut, and the immediate roof of the point with the greatest rut on a planet is the point with the greatest jut.

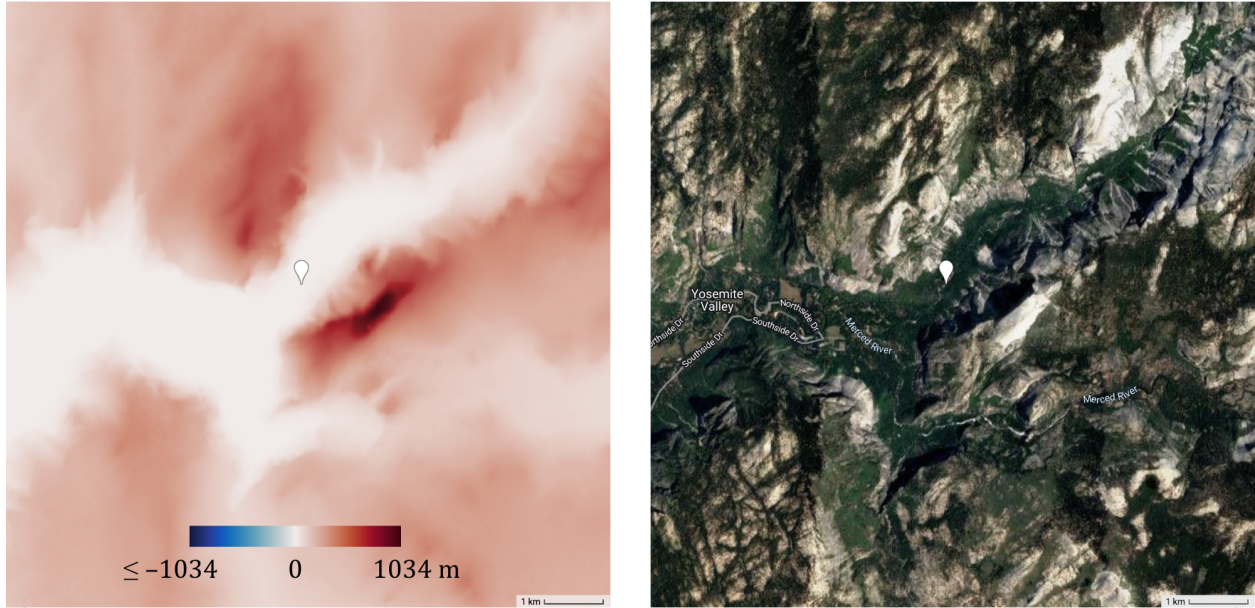


Figure 12: Diverging angle-reduced height map of Mirror Lake. The rut of Mirror Lake is the maximum value, 1034 m, measured at its immediate roof at the top of Half Dome.

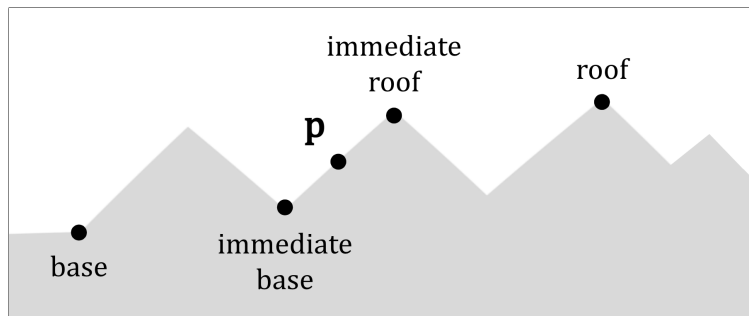


Figure 13: In this simplified landscape, the base and roof of \mathbf{p} are the lowest and highest points of the mountain range that \mathbf{p} is in, while its immediate base and immediate roof are the lowest and highest points of the mountain that \mathbf{p} is on.

3.5 Composite Point Measures

The aforementioned point measures can be combined to describe more aspects of relief. Below are some examples:

3.5.1 Range

The *range* of point \mathbf{p} is the sum of its dominance and submission:

$$\text{ran}(\mathbf{p}) = \text{dom}(\mathbf{p}) + \text{sub}(\mathbf{p})$$

Range measures the total span of vertical relief in the curvature-scale surroundings of a point. It yields similar values for points in close proximity. When applied to a point

within a mountain range, range typically describes the span of vertical relief in the mountain range. For example, the range of the summit of Half Dome is the sum of its dominance and submission, $2235 \text{ m} + 1252 \text{ m} = 3487 \text{ m}$, an indicator of the span of vertical relief in the Yosemite region of the Sierra Nevada. By virtue of being in close proximity, the range of Mirror Lake is almost the same, with a value of $809 \text{ m} + 2682 \text{ m} = 3491 \text{ m}$.

3.5.2 Normalized Dominance

The *normalized dominance* of point \mathbf{p} is its dominance divided by its range:

$$\text{ndom}(\mathbf{p}) = \frac{\text{dom}(\mathbf{p})}{\text{ran}(\mathbf{p})}.$$

Normalized dominance yields a value ranging from 0 at a submissive point to 1 at a dominant point, describing the vertical position of a point within the range of vertical relief in its curvature-scale surroundings.⁶ Continuing the running example of Yosemite National Park: At the city of Merced in the Central Valley, the normalized dominance is 0.02. Moving higher to Mirror Lake in Yosemite Valley, the normalized dominance is 0.23. At the summit of Half Dome, the normalized dominance is 0.64. Finally, at the summit of Mt. Dana, a dominant point, the normalized dominance is 1.

3.5.3 Fluctuation

The *fluctuation* of point \mathbf{p} is the sum of its jut and rut:

$$\text{fluc}(\mathbf{p}) = \text{jut}(\mathbf{p}) + \text{rut}(\mathbf{p})$$

Fluctuation measures how mountainous the surroundings of a point are, accounting for height differences and steepness in both the upwards and downwards directions of the point. For a point within a mountain range, its fluctuation usually approximates the angle-reduced height of a neighboring mountaintop with respect to a neighboring valley, thus describing mountaintop-to-valley relief (as opposed to relief in the entire mountain range, as described by range). For instance, the fluctuation of Mt. Whitney trailhead at Whitney Portal is equal to the sum of its jut and rut: $134 \text{ m} + 680 \text{ m} = 814 \text{ m}$. By being on the same slope of Mt. Whitney, Upper Boy Scout Lake has a similar fluctuation: $376 \text{ m} + 465 \text{ m} = 841 \text{ m}$.

3.5.4 Normalized Jut

The *normalized jut* of point \mathbf{p} is its jut divided by its fluctuation:

$$\text{njut}(\mathbf{p}) = \frac{\text{jut}(\mathbf{p})}{\text{fluc}(\mathbf{p})}$$

Normalized jut yields a value from 0 to 1 that describes the vertical position of a point relative to its immediate surroundings.⁷ The normalized jut of a point within a mountain

⁶Normalized dominance is also equal to $1 - \frac{\text{sub}(\mathbf{p})}{\text{ran}(\mathbf{p})}$.

⁷Normalized jut is also equal to $1 - \frac{\text{rut}(\mathbf{p})}{\text{fluc}(\mathbf{p})}$.

range typically describes the vertical position of the point relative to the mountain it is located on (rather than vertical position relative to the mountain range, as for normalized dominance) in a perceptually accurate way. Unlike normalized dominance, normalized jut is usually close to 1 at the top of a mountain and close to 0 at the bottom of a valley, regardless of the vertical position of the mountain or valley relative to a mountain range. In addition, normalized jut gives greater weight to steeper slopes of a mountain. For instance, if \mathbf{p} is, say, vertically halfway on a mountain with a steeper top half and a more gradual bottom half, the normalized jut of \mathbf{p} would be less than $\frac{1}{2}$.

As an example, the normalized jut of Mather Point on the South Rim of the Grand Canyon is equal to its jut divided by its fluctuation, $\frac{710\text{m}}{723\text{m}} = 0.98$. The value close to 1 describe the vertical position of Mather Point relative to its immediate surroundings in a perceptually accurate way. (In contrast, the normalized dominance of Mather Point is only 0.58 because the distant San Francisco Peaks rise above its horizontal plane.) Another example is Whitney Portal, with an angle-reduced normalized dominance of $\frac{138\text{m}}{819\text{m}} = 0.16$. The low value makes sense from a perceptual standpoint, given that Whitney Portal is the usual starting point of the Mt. Whitney ascent, and that the drive up to Whitney Portal is not nearly as steep as the ascent to the summit. (Meanwhile, Whitney Portal's normalized dominance of 0.53 suggests that it is positioned approximately halfway within the span of relief in the Sierra Nevada mountain range.)

3.5.5 Domangle

The *domangle* of point \mathbf{p} is equal to the following:

$$\theta_{\text{dom}}(\mathbf{p}) = \arcsin\left(\frac{\text{jut}(\mathbf{p})}{\text{dom}(\mathbf{p})}\right)$$

Domangle measures yields a value from 0° to 90° that describes how steeply a point rises above its surroundings. It provides an interpolated value between the angle of elevation of \mathbf{p} above its base and its angle of elevation above its immediate base. Taking Yosemite as an example, the domangle of the summit of Half Dome is its jut divided by its dominance, $\arcsin\left(\frac{1093\text{m}}{2235\text{m}}\right) = 29.3^\circ$. While one might expect a greater value given how steeply Half Dome rises above Yosemite Valley, domangle also factors in the higher but less steep rise of Half Dome above the Central Valley, providing an interpolated value between these two. In fact, Half Dome has a significantly higher domangle than most summits. In comparison, the domangle of the summit of Mt. Lyell, the highest point in Yosemite National Park, is $\arcsin\left(\frac{309\text{m}}{3367\text{m}}\right) = 5.3^\circ$. Despite having a higher dominance than Half Dome, Mt. Lyell rises much more gradually.

3.5.6 Subangle

The *subangle* of point \mathbf{p} is equal to the following:

$$\theta_{\text{sub}}(\mathbf{p}) = \arcsin\left(\frac{\text{rut}(\mathbf{p})}{\text{sub}(\mathbf{p})}\right)$$

Subangle yields a value from 0° to 90° that describes how steeply a point dips below its surroundings. Its value is between the angle of elevation of the roof of \mathbf{p} above \mathbf{p} and the

angle of elevation of its immediate roof. For instance, the subangle of Mirror Lake is equal to its rut divided by its submission, $\arcsin\left(\frac{1034\text{m}}{2682\text{m}}\right) = 22.7^\circ$. While one might expect a higher value given how steeply Half Dome rises above Mirror Lake, subangle also factors in the less steep rise of the higher peaks east of Half Dome. In comparison, the subangle of the summit of Half Dome is only $\arcsin\left(\frac{68\text{m}}{1252\text{m}}\right) = 3.1^\circ$, as Half Dome does not dip steeply below higher mountains nearby.

3.5.7 Rangle

The *rangle* of point \mathbf{p} is equal to the following:

$$\theta_{\text{ran}}(\mathbf{p}) = \arcsin\left(\frac{\text{fluc}(\mathbf{p})}{\text{ran}(\mathbf{p})}\right)$$

Rangle yields a value from 0° to 90° that describes the overall steepness of the surroundings of a point in both the upwards and downwards directions, weighted towards the direction of greater curvature-scale relief. The rangle of a point is between its domangle and subangle. As an example, the rangle of the summit of Half Dome is its fluctuation divided by its range, $\arcsin\left(\frac{1161\text{m}}{3487\text{m}}\right) = 19.4^\circ$. The rangle of Half Dome is weighted more towards its domangle, as the dominance of Half Dome is greater than its submission.

3.6 Domain-Restricted Point Measures

Occasional tasks may call for including only certain points in the planetary surface when calculating the datumless point measures. Examples include the jut of Mt. Everest with respect to its Nepal side (ignoring points on the Tibetan side), or the dry submission of an underwater point with respect to the sea floor (ignoring points on land).

Let T be a subset of the planetary surface ($T \subset S$) representing the region that S is being restricted to. Let f be the point measure whose domain-restricted form is of interest, and let $f(\mathbf{p}, T)$ denote the domain-restricted form of f with respect to T .

If f is a non-composite measure (i.e., dominance, submission, jut, or rut), $f(\mathbf{p}, T)$ is equivalent to the result of taking the maximum with respect to all points in T , rather than all points in S . For example:

$$\text{dom}(\mathbf{p}, T) = \max_{\mathbf{q} \in T} z_{\mathbf{p} \leftarrow \mathbf{q}}$$

Meanwhile, if f is a composite measure, $f(\mathbf{p}, T)$ is equivalent to the result of replacing all non-composite point measures in the formula for f by their domain-restricted forms. For example:

$$\text{ndom}(\mathbf{p}, T) = \frac{\text{dom}(\mathbf{p}, T)}{\text{ran}(\mathbf{p}, T)} = \frac{\text{dom}(\mathbf{p}, T)}{\text{dom}(\mathbf{p}, T) + \text{sub}(\mathbf{p}, T)}$$

4 Datumless Surface Measures

The datumless surface measures reveal various aspects about the relief and surface characteristics of a region, as opposed to that of a single point.

4.1 Preliminaries: Datumless Surface Functionals

The datumless surface functionals (not to be confused with the datumless surface measures) are datumless formulations of surface area, mean value of a surface variable, and other statistics of a surface variable, all of which can be applied directly to the planetary surface without projecting it onto an arbitrary reference ellipsoid. However, quite conveniently, the datumless surface functionals on most roughly spherical planets measure a similar value as their analogues on a reference ellipsoid, and can be approximated as such in a geographic information system (GIS) program. The datumless surface functionals are not limited to topographic applications, and can be applied outside the field.

4.1.1 Datumless Surface Area

Due to the fractal-like texture of the planetary surface, it does not make sense to calculate its surface area directly. Instead, the most common pre-existing way of representing surface area involves projection onto a reference ellipsoid. While convenient, the requirement of a datum makes this approach arbitrary to an extent.

Meanwhile, consider the equipotential surfaces, or surfaces of constant gravitational potential. The equipotential surfaces are physically meaningful surfaces with a defined surface area. In addition, there is a one-to-one correspondence between points in S and points on an equipotential surface. This is because points in S can be moved along their plumbines to their corresponding locations on an equipotential surface. One may think of choosing a particular equipotential surface to represent the surface area of a planet. However, such an approach is still arbitrary, as the choice of which equipotential surface to use remains open-ended.

The non-arbitrary solution is to not have to choose a particular equipotential surface, but instead to add up the surface areas of bits and pieces of the equipotential surfaces that intersect the planetary surface. Let T be a subset of the planetary surface ($T \subseteq S$) denoting the region whose surface area is of interest. The *datumless surface area* of T , denoted by $\text{DSA}(T)$, is the sum of the surface areas of infinitesimally small portions of different equipotential surfaces that intersect T . Datumless surface area can be notated by the coarea formula in geometric measure theory [8]:

$$\text{DSA}(T) = \int_T |\nabla U(\mathbf{p})| d\mathbf{p}$$

where $U(\mathbf{p})$ denotes the gravitational potential at point \mathbf{p} .

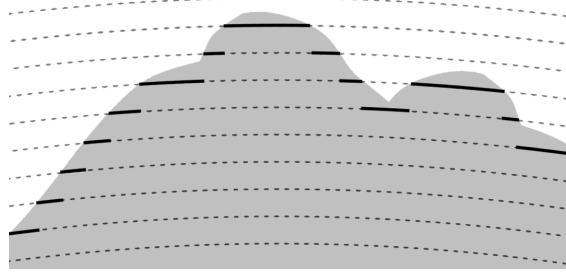


Figure 14: Datumless surface area can be approximated by adding up the surface areas of portions of equipotential surfaces that intersect the planetary surface, outlined in black in this diagram.

4.1.2 Datumless Mean Value

Let f be a function that assigns points on the planetary surface S to numerical values. Examples of such functions include surface temperature, precipitation, and in the case of this paper, the datumless point measures. The *datumless mean value* of f over the region T , denoted by $\bar{f}(T)$, is the sum of the products of the surface areas of infinitesimally small portions of T -intersecting equipotential surfaces with the values of f at their respective locations, all of which is divided by the datumless surface area of T :

$$\bar{f}(T) = \frac{1}{\text{DSA}(T)} \int_T f(\mathbf{p}) |\nabla U(\mathbf{p})| d\mathbf{p}$$

4.1.3 Other Datumless Statistics

While its applications are outside the scope of this paper, it is possible to construct a frequency distribution of the values that f can take on within a region. This allows the representation of other statistics beyond mean value, such as standard deviation, median, and quantiles.

Let $T_{f \leq x}$ denote the subset of T consisting of all points in T where $f(\mathbf{p})$ is less than or equal to x :

$$T_{f \leq x} = \{\mathbf{p} \in T \mid f(\mathbf{p}) \leq x\}$$

The *datumless percentile* of the value x for the surface function f on region T , denoted by $\text{DPC}(x, f, T)$, is equal to the following:

$$\text{DPC}(x, f, T) = \frac{\text{DSA}(T_{f \leq x})}{\text{DSA}(T)}$$

Using datumless percentile, one can construct a *datumless frequency distribution* of the values of f within T by calculating the datumless percentile of all values of f within T .⁸ From the datumless frequency distribution, a variety of *datumless statistics* can be derived.⁹

⁸Note that more computationally efficient ways of constructing a datumless frequency distribution may exist; this is only a proof of concept.

⁹Concepts in the datumless surface functionals can also be applied to paths on the planetary surface that are locally one-dimensional. In such cases, datumless surface area becomes datumless path length instead.

4.2 Datumless Surface Measures: Special Considerations

The *datumless surface measures* describe various aspects about the relief and surface characteristics within a region, as opposed to that of a single point. They are essentially the mean values of the datumless point measures, with a few caveats and special considerations:

4.2.1 Domain-Restricted Surface Measures

Let f be the point measure whose mean value over region T is being represented. If f is non-domain-restricted, its mean value over T is notated as $\bar{f}(T)$. However, if f is domain-restricted over region G , its mean value over T is notated as $\bar{f}(T, G)$. The most common form of domain restriction regarding the datumless surface measures is to restrict the domain of f to T , the region whose mean value is being calculated. This is notated as $\bar{f}(T, T)$.

For instance, let T denote the subset of the planetary surface consisting of all points in the Central Valley of California. The mean submission of Central Valley (with respect to the planetary surface), denoted by $\overline{\text{sub}}(T)$, is well over 1000 m, as the Sierra Nevada and Coast Ranges rise significantly above the region. However, the mean submission of Central Valley with respect to itself, denoted by $\overline{\text{sub}}(T, T)$, is much closer to 0, as the region itself is fairly flat.

4.2.2 Special Definition for Composite Surface Measures

If f is a composite point measure, \bar{f} is not simply the mean value of f over all points in T . Instead, it is defined as being equivalent to the result of replacing all non-composite point measures in the formula for f by their mean values over T . For example:

$$\overline{\text{ndom}}(T) = \frac{\overline{\text{dom}}(T)}{\overline{\text{ran}}(T)} = \frac{\overline{\text{dom}}(T)}{\overline{\text{dom}}(T) + \overline{\text{sub}}(T)}$$

The same applies to domain-restricted surface measures. For example:

$$\bar{\theta}_{\text{ran}}(T, T) = \frac{\overline{\text{fluc}}(T, T)}{\overline{\text{ran}}(T, T)} = \frac{\overline{\text{jut}}(T, T) + \overline{\text{rut}}(T, T)}{\overline{\text{dom}}(T, T) + \overline{\text{sub}}(T, T)}$$

4.3 Measuring Surface Characteristics

This subsection describes the appropriate datumless surface measures to use to quantify different surface characteristics, namely ruggedness, steepness, skewness, and kurtosis. The datumless surface measures are inspired by the surface roughness parameters in mechanical engineering [4].

4.3.1 Curvature-Scale vs. Immediate Relief

Depending on the resolution at which relief is to be assessed, different datumless surface measures should be used.

The *curvature-scale relief* of a region is concerned with the shape, size, and structure of large-scale features such as mountain ranges and plains. Measures of curvature-scale relief include mean dominance, mean submission, mean range, and mean normalized dominance.

Meanwhile, the *immediate relief* of a region is concerned with the shape, size, and structure of neighboring small-scale features, such as mountains and valleys within a mountain range. Measures of immediate relief include mean jut, mean rut, mean fluctuation, and mean normalized jut.

4.3.2 Rise, Dip, and Span-Based Relief

Certain datumless surface measures may be more appropriate than others, depending on the unique geomorphic processes within the region of interest.

Rise-based surface measures equate relief with rise above local terrain. They include mean dominance, mean jut, and mean domangle. Rise-based surface measures make the most sense in places when the main geomorphic processes tend to generate mostly protruding features. This is true for much of Earth, as the planet's unique plate tectonics enable the formation of extensive mountain ranges.

Dip-based surface measures equate relief with dip below local terrain. They include mean submission, mean rut, and mean subangle. Dip-based surface measures make the most sense in places where the main geomorphic processes tend to generate mostly recessed features. Such locations include ocean trenches on Earth and the Valles Marineris canyon on Mars.

Span-based surface measures equate relief with both rise above and dip below local terrain, giving equal weight to rises and dips of the same magnitude. Span-based surface measures include mean range, mean fluctuation, and mean range. The span-based approach makes sense in places with a fairly balanced degree of protruding and recessed features. On Earth, that includes certain highland and mesa regions such as the Colorado Plateau and the Ethiopian Highlands. Span-based surface measures should be used in places heavily shaped by asteroid impacts, which tend to generate both recessed crater floors and protruding crater rims. Such locations include much of the Moon and most other planets, which lack the plate tectonics unique to Earth. In addition, span-based measures are recommended for comparing the degree of relief across different planets with differing geomorphic processes.

4.3.3 Ruggedness Measures

In this paper, *ruggedness* refers to the degree of vertical relief within a region. The most common pre-existing method of quantifying ruggedness involves taking an average of elevation or an elevation-derived measure. However, elevation not only requires a datum, but also does not directly describe local relief, unlike the datumless measures.



Figure 15: Visualization of ruggedness.

Within the datumless framework, curvature-scale ruggedness is quantified by mean dominance (rise-based), mean submission (dip-based), and mean range (span-based).

In the meantime, immediate ruggedness is quantified by mean jut (rise-based), mean rut (dip-based), and mean fluctuation (span-based). The immediate ruggedness measures are useful for capturing the impressiveness of a mountainous region, as they account for both height differences and steepness between neighboring mountains and valleys.

4.3.4 Steepness Measures

Outside the datumless framework, slope is often used to quantify the steepness of a point's surroundings and averaged to determine the steepness of a region. Nevertheless, slope is wholly dependent on the resolution of a surface model and fails to provide meaningful values at very high resolutions.

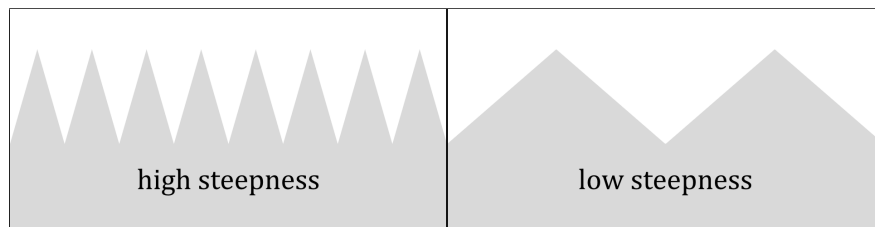


Figure 16: Visualization of steepness.

Within the datumless framework, mean domangle (rise-based), mean subangle (dip-based), and mean range (span-based) are used to quantify the steepness of a region. They provide an interpolated value between the angle of elevation of a typical point relative to its immediate surroundings and the angle of elevation of a typical point relative to its curvature-scale surroundings.

4.3.5 Skewness Measures

In this paper, *skewness* refers to the balance between low and high terrain. A region is low-skewed if it consists predominantly of low terrain, and high-skewed if it consists predominantly of high terrain. For instance, a mostly flat region with widely-separated mountain ranges is low-skewed, whereas a mostly flat region with widely-separated valleys is high-skewed.

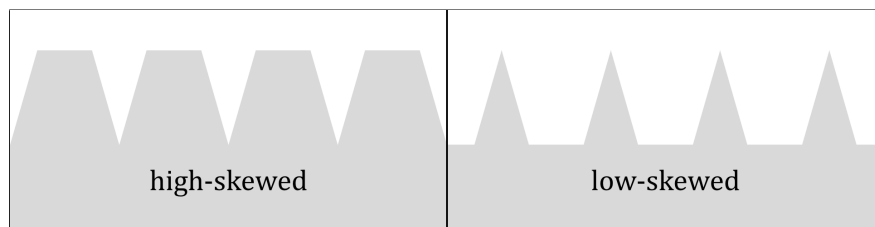


Figure 17: Visualization of skewness.

Within the datumless framework, curvature-scale skewness is quantified by mean normalized dominance, with a value close to 0 indicating a low skew and a value close to 1 indicating a high skew. On the curvature-scale, Earth is especially low-skewed compared to other planets, as due to its unique plate tectonics, mountain ranges are its most common source of relief. In comparison, the Moon has much more of a neutral skew, as its asteroid impacts tend to generate a similar degree of protruding and recessed features.

Meanwhile, immediate skewness is quantified by mean normalized jut, with a value close to 0 indicating low-skewed terrain and a value close to 1 indicating high-skewed terrain. Immediate skewness is determined by the shape of neighboring mountains and valleys. For instance, a landscape of pointy mountains separated by U-shaped valleys has a low skew, whereas a landscape of flat-topped mountains separated by narrow valleys has a high skew.

4.3.6 Kurtosis Measures

In this paper, *kurtosis* refers to the tendency of terrain to gravitate to high and low extremes. A region has a high kurtosis if points within it often gravitate to such extremes, and a low kurtosis if points within it tend to stay close to the middle of the local span of relief.

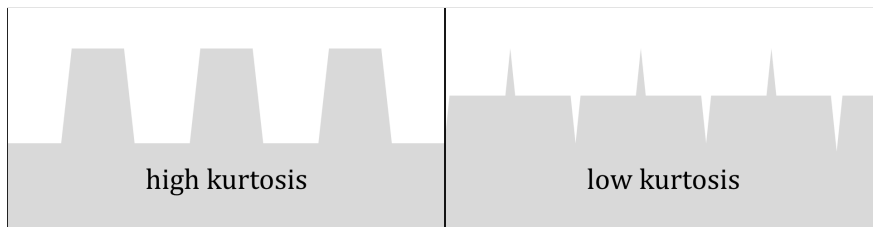


Figure 18: Visualization of kurtosis.

Kurtosis measures require a few preliminaries before arriving at their main definitions. The measure of curvature-scale kurtosis is defined as follows:

- Let the *deviation* of point \mathbf{p} be equal to half its range minus its submission. Deviation describes how far a point is from central tendency on the curvature-scale.

$$\text{dev}(\mathbf{p}) = \frac{\text{ran}(\mathbf{p})}{2} - \text{sub}(\mathbf{p}) = \frac{\text{dom}(\mathbf{p}) - \text{sub}(\mathbf{p})}{2}$$

- Let the *mean absolute deviation* (MAD) of region T be equal to the mean value of the absolute value of deviation $|\text{dev}(\mathbf{p})|$ over region T , without applying the special definition of mean value for composite point measures.¹⁰

$$\text{MAD}(T) = \frac{1}{\text{DSA}(T)} \int_T |\text{dev}(\mathbf{p})| |\nabla U(\mathbf{p})| d\mathbf{p}$$

The measure of kurtosis based on these preliminaries is called *normalized mean absolute deviation* (NMAD), which is equal to the mean absolute deviation of T divided by half the

¹⁰Mean absolute deviation can also be used to measure curvature-scale ruggedness.

mean range of T :

$$\text{NMAD}(T) = \frac{\text{MAD}(T)}{\overline{\text{ran}}(T)/2} = \frac{2(\text{MAD}(T))}{\overline{\text{ran}}(T)}$$

Normalized mean absolute deviation yields a value from 0 to 1, with a higher value indicating greater kurtosis on the curvature-scale.

Meanwhile, the measure of immediate kurtosis is defined via a similar process:

- Let the *perturbation* of point \mathbf{p} be equal to half its fluctuation minus its rut. Perturbation describes how far a point is from central tendency relative to its immediate surroundings.

$$\text{pert}(\mathbf{p}) = \frac{\text{fluc}(\mathbf{p})}{2} - \text{rut}(\mathbf{p}) = \frac{\text{jut}(\mathbf{p}) - \text{rut}(\mathbf{p})}{2}$$

- Let the *mean absolute perturbation* of region T , denoted by $\text{MAP}(T)$, be equal to the mean value of the absolute value of perturbation $|\text{pert}(\mathbf{p})|$ over region T , without applying the special definition for composite surface measures.¹¹

$$\text{MAP}(T) = \frac{1}{\text{DSA}(T)} \int_T |\text{pert}(\mathbf{p})| |\nabla U(\mathbf{p})| d\mathbf{p}$$

The *normalized mean absolute perturbation* of region T , denoted by $\text{NMAP}(T)$, is equal to the mean absolute perturbation of T divided by half the mean fluctuation of T :

$$\text{NMAP}(T) = \frac{\text{MAP}(T)}{\overline{\text{fluc}}(T)/2} = \frac{2(\text{MAP}(T))}{\overline{\text{fluc}}(T)}$$

Normalized mean absolute perturbation yields a value from 0 to 1, with a higher value indicating greater immediate kurtosis.

The domain-restricted forms of the kurtosis measures are revealed by replacing all instances of (\mathbf{p}) in the previous expressions by (\mathbf{p}, T) and all instances of (T) by (T, G)

5 Computing the Datumless Point Measures on Earth and Beyond

This section introduces formulas that can be directly applied in a GIS program to compute the datumless point measures. It also showcases the values of the datumless point measures at various locations on Earth, Moon, Mars, and Vesta, comparing their values with elevation and prominence. The datumless surface measures are not computed due to issues of high time complexity.

¹¹Mean absolute perturbation can also be used to measure immediate ruggedness.

5.1 Computing the Datumless Point Measures

5.1.1 Converting a Surface Model to ECEF

The first step in computing the datumless point measures is to convert an existing surface model such as a DEM to an ECEF coordinate system. The following models are used for their respective planets:

Table 1: Surface models used for their respective planets.

Planet	Model	Height Type	Resolution
Earth (land and water surface)	ALOS World 3D [9]–[12]	Orthometric	30 m
Earth (bathymetry)	GEBCO_2022 Grid [13]	Orthometric	450 m
Earth (geoid)	EGM96 [14], [15]	Geoid	450 m
Moon	LRO LOLA [16]	Ellipsoidal	118 m
Mars (orthometric)	MOLA - HRSC Blended [17]	Orthometric	200 m
Mars (areoid)	GMM-2B [18]	Areoid	200 m
Vesta	Dawn FC HAMO [19]	Radius	93 m

On Earth and Mars, elevation is presented as orthometric height, or height above the geoid—namely, the EGM96 geoid on Earth and the GMM-2B areoid (essentially a Martian geoid with an arbitrarily defined geopotential) on Mars. Before converting to ECEF, it is a good practice to convert orthometric height to height above a reference ellipsoid—the WGS84 reference ellipsoid on Earth and a sphere with a 3,396,190 m radius on Mars.¹² The following equation is used for this conversion:

$$h = H + N$$

where h denotes ellipsoidal height, H denotes orthometric height, and N denotes geoid height, i.e., the height of the geoid above the reference ellipsoid. The EGM96 geoid model and GMM-2B areoid model[18] are used for N on Earth and Mars, respectively. This conversion on Mars is done with the help of Ames Stereo Pipeline [20].

The next step is converting ellipsoidal height to X , Y , and Z coordinates in ECEF using the following equations [21]:

$$\phi = \text{latitude}$$

$$\lambda = \text{longitude}$$

$$h = \text{ellipsoidal height}$$

$$a = \text{length of equatorial radius of reference ellipsoid}$$

$$b = \text{length of polar radius of reference ellipsoid}$$

$$f = 1 - \frac{b}{a}, \text{ the flattening of the ellipsoid}$$

$$e^2 = 2f - f^2$$

¹²The usage of a reference ellipsoid in this case is non-arbitrary, as it is for approximating the direction of gravity—a meaningful physical concept—rather than for providing an arbitrary datum to quantify relief.

$$\begin{aligned}
N(\phi) &= \frac{a}{\sqrt{1 - e^2 \sin^2 \phi}} \\
X &= (N(\phi) + h) \cos \phi \cos \lambda \\
Y &= (N(\phi) + h) \cos \phi \sin \lambda \\
Z &= ((1 - e^2) N(\phi) + h) \sin \phi
\end{aligned}$$

The values of a and f used for their respective planets are listed in the table below; b is derivable from a and f . Heights in the Vesta model, provided as radius from the center of mass, can be treated as height above an ellipsoid with dimensions $a = 0$ and $f = 0$.

Table 2: Values of a and f used for their respective planets.

Planet	a	f
Earth	6,378,137 m	1 / 298.257223563
Moon	1,737,400 m	0
Mars	3,396,190 m	0
Vesta	0 m	0

5.1.2 Approximating the Vertical Unit Vector

After converting a DEM to ECEF, the next step is to compute the vertical unit vector for points on the planetary surface.

On Earth and Mars, the vertical unit vector can be approximated to point normal to their respective geoid and areoid models, which are created to model an equipotential surface. Using a GIS software, one can compute the angles for the slope α and aspect β of a geoid or areoid model. (Aspect is an angle from 0° to 360° describing the direction that the slope faces, with 0° denoting a north-facing slope and an increasing angle corresponding to a clockwise rotation on the compass rose.) Given the slope and aspect of the geoid or areoid at a particular latitude-longitude pair, the vertical unit vector at that location is calculated as follows:

$$\begin{aligned}
&R_z(\lambda) \times R_y(-\phi) \times R_x(-\beta) \times R_y(-\alpha) \times \begin{pmatrix} 1 \\ 0 \\ 0 \end{pmatrix} \\
&= \begin{pmatrix} (\cos \alpha \cos \phi - \sin \alpha \cos \beta \sin \phi) \cos \lambda - \sin \alpha \sin \beta \sin \lambda \\ (\cos \alpha \cos \phi - \sin \alpha \cos \beta \sin \phi) \sin \lambda + \sin \alpha \sin \beta \cos \lambda \\ \cos \alpha \sin \phi + \sin \alpha \cos \beta \cos \phi \end{pmatrix}
\end{aligned}$$

where the R 's denote 3-dimensional rotation matrices.

On the Moon, where a geoid model not readily available, the vertical unit vector can be approximated to point normal to the reference ellipsoid. Since the reference ellipsoid is a perfect sphere on both planets, the vertical unit vector also points directly away from the planet's center of mass. Given the latitude and longitude of a point, its vertical unit vector normal to the reference ellipsoid is calculated as follows:

$$\hat{\mathbf{k}} = R_z(\lambda) \times R_y(-\phi) \times \begin{pmatrix} 1 \\ 0 \\ 0 \end{pmatrix} = \begin{pmatrix} \cos \phi \cos \lambda \\ \cos \phi \sin \lambda \\ \sin \phi \end{pmatrix}$$

On Vesta, a reference ellipsoid of dimensions $a=285$ km and $b=229$ km has been previously used by NASA [22]. However, there lacks a convenient way to convert distance from the center of mass (as provided by the Vesta surface model) to latitude and longitude on the NASA ellipsoid. Therefore, the vertical unit vector on Vesta is approximated with a different approach: Consider the existence of concentric ellipsoids with the same center and the same proportions (i.e., the same a/b ratio) as the NASA ellipsoid. The vertical unit vector of a point is approximated as pointing normal to the concentric ellipsoid that it touches. Given the X , Y , and Z coordinates of a point on Vesta in ECEF, its vertical unit vector $\hat{\mathbf{k}}$ is approximated as follows:

$$\mathbf{k} = \begin{pmatrix} X / a^2 \\ Y / a^2 \\ Z / b^2 \end{pmatrix}$$

$$\hat{\mathbf{k}} = \frac{\mathbf{k}}{|\mathbf{k}|}$$

After computing the ECEF coordinates and vertical unit vectors of points on the planetary surface, standard GIS operations can be used to compute all other quantities related to the datumless point measures. To save computational time, the aforementioned computations only need to be applied to points within the curvature-scale surroundings of \mathbf{p} , as points very far away are irrelevant to the calculation of the datumless point measures.

5.2 Datumless Point Measures on Earth and Beyond

Google Earth Engine [7] is used to compute all values of the datumless point measures in this paper, along with generating all maps. Measured points are located with the help of Google Maps [23]. Summit elevation and prominence values on Earth are either found on Peakbagger.com [24] or derived manually from a DEM, with the exception of the dry prominence of Mauna Kea, which is found in [25]. Measurements and related conclusions are subject to change and should always be verified.

5.2.1 Earth

Earth’s topography is unique among the planets in the Solar System. Unlike most planets, its unique plate tectonics play a major role in generating mountain ranges.

An interesting global phenomenon to note is that mountains closer to polar latitudes along with those with a higher base elevation tend to measure greater a jut for their dominance, i.e., a greater domangle. This is likely due to the effects of glacial erosion in sculpting steeper mountains [26]. Closer to the poles, lower temperatures allow steep, glacier-carved flanks to extend to lower terrain, typically resulting in immediate bases being close to the bottom of a mountain range. Meanwhile, closer to the equator, glaciers are only supported in high altitudes, usually resulting in immediate bases being higher up within the mountain range that a point resides in.

In the contiguous U.S., the highest dominance values are found in the Sierra Nevada and the Cascade Range, with a handful of summits measuring above 3500 m and Mt. Rainier being the only to measure above 4000 m. Despite having a similar elevation, the Rocky Mountains have a lower dominance as a result of rising from higher plains, with the greatest

values in the American Rockies only slightly exceeding 2500 m. Places with a jut exceeding 1000 m include the Teton Range, Glacier National Park, Half Dome, Mt. San Jacinto, the North Cascades, and last but not least, Mt. Rainier, which has the highest dominance and jut¹³ of any major summit—hereby denoting a peak with at least 300 m of prominence—in the contiguous United States. Within the Rocky Mountains, the subranges of Colorado are generally less steep than their more northerly neighbors, with the most impressive¹⁴ summits in the state measuring a jut between 500 m and 750 m. In comparison to all of these places, the Appalachian Mountains feature significantly less relief as a result of old age, with all locations measuring below 2000 m of dominance and 500 m of jut.

In the rest of North America, the Canadian Rockies measure a similar dominance as their American counterparts but a significantly higher jut and domangle. Jut values of over 1500 m are common in the region, culminating at Mt. Robson, which has over 1900 m of jut. The highest and most impressive features in North America are found in Alaska and Northwest Canada, with Denali measuring the highest dominance of over 5500 m and Mt. St. Elias measuring the highest jut of over 2500 m. Mountains in Mexico tend to have a lower domangle, likely due in part to decreased glaciation. Pico de Orizaba stands out as the only major summit in the country with over 5000 m of dominance and over 1000 m of jut, with a few other stratovolcanoes measuring above 4000 m of dominance.

South America is home to the Andes, the highest mountain range outside of Asia in terms of both dominance and elevation. Within the Andes, a handful of major summits have a dominance of over 5500 m, with Aconcagua measuring the greatest dominance of over 6000 m. The greatest jut values in the Andes are just over 1800 m. The Southern Andes have the highest domangle, likely due to glaciation at lower altitudes due to the colder climate. In fact, the jut of major summits in Patagonia are comparable to those of the Central and Northern Andes, which have almost twice the dominance. Meanwhile, the Central Andes, which correspond to the Atacama Desert and the Altiplano, tend to measure the lowest domangle values in the entire mountain range, which could in part be due to aridity limiting the formation of glaciers [27].

In Africa, mountains tend to measure a lower jut and domangle than most other continents, likely due in part to decreased glaciation. The highest and most impressive mountain in the continent is Kilimanjaro, with a dominance of just over 5000 m and a jut of just over 1300 m. A few other major summits in Africa measure a dominance of over 4000 m. A mountain that demonstrates the sculpting effects of glaciers particularly well is Mt. Kenya. The extinct stratovolcano rises very gradually from its base, all the way up to a height where glaciers can be supported, where it then rises abruptly to the summit. The immediate base of Mt. Kenya is located right where this transition occurs, while its base located where the mountain's lower, more gradual slopes meet flat plains.

In Europe, the two highest mountain ranges are the Alps and Caucasus Mountains. Within the Alps, several major summits exceed 4000 m of dominance, with Mont Blanc measuring the highest dominance of just over 4400 m. The Alps have a remarkably high jut for their dominance, with numerous locations measuring over 1000 m of jut and a few

¹³For convenience, the jut of a mountain will refer to its summit measurement, even though non-summit locations may measure a higher jut.

¹⁴The term *impressive* is used objectively to denote a high jut.

locations near Mont Blanc measuring over 1500 m. Compared with the Alps, the Caucasus Mountains have slightly higher dominance values, with a few mountains measuring between 4500 m and 5000 m, including Mt. Elbrus, the mountain with the highest dominance in Europe. However, the Caucasus also generally have a slightly lower jut compared to the Alps, with the most impressive mountains measuring between 1000 m and 1500 m of jut and no mountain exceeding 1500 m.

Asia is home to the most rugged terrain on Earth. The greatest values of dominance and jut on the planet are found in a region bounded roughly by the Tian Shan to the north, the Himalaya to the south, the Hengduan Mountains to the east, and the Pamir-Alay to the west. Within this region, numerous major summits have a dominance of over 6000 m and a jut of over 2000 m. In terms of dominance, the Himalaya is the highest mountain range of them all, with dominance values exceeding 7000 m at a handful of major summits. Mount Everest measures the highest dominance on the planet with a value of 8081 m, measured from its base at the bottom of the Himalaya where it meets the Indo-Gangetic Plain. Second and third place for major summits with the highest dominance are Kangchenjunga and Lhotse. Meanwhile, K2 barely exceeds 5500 m of dominance, as the Karakoram mountain range sits on a high plateau. However, both the Himalaya and Karakoram are home to summits exceeding 2500 m of jut and occasionally 3000 m. The greatest jut of any major summit goes to Nanga Parbat, with a value of over 3100 m, measured from its immediate base at the bottom of its massive Rupal Face, often regarded as the tallest in the world. Asia is also home to the Tibetan Plateau, which is so large that the base of mountains in its central parts are measured directly from the plateau, rather than from the low plains that the plateau rises from. The dominance of mountains in the interior of the Tibetan Plateau tend to be quite high, likely as a result of altitude-induced glaciation.

In Oceania, the mountain with the greatest dominance is Puncak Jaya, measuring a dominance of just over 4800 m. The entire landmass of Australia is considerably flat, with Mt. Kosciuszko, its highest-dominance feature, measuring a dominance of just below 2000 m, and all locations measuring below 400 m of jut. In contrast, neighboring New Zealand features significantly greater relief. The highest dominance in New Zealand is measured atop Aoraki / Mt. Cook, with a value of just over 3600 m. The glacier-carved fjords of Milford Sound have some of the highest jut values in the world for their dominance, with Mitre Peak measuring a jut of over 1300 m, similar to that of the Matterhorn which has over twice the dominance.

In Antarctica, the Sentinel Range is the highest mountain range, with Vinson Massif measuring the highest dominance of just over 4500 m and a few locations measuring a jut of over 1500 m. Moving inland, the ice sheet thickens so gradually that points in its central portions measure a dominance and jut close to 0, despite having thousands of meters of elevation. A similar phenomenon occurs in the center of the ice sheet of Greenland.

Regarding suboceanic features, the dry datumless measures directly describe their relief relative to the ocean floor, providing a convenient alternative to elevation, whose values need to be compared with other elevation values for this purpose. The greatest dry dominance on Earth is measured atop an unnamed seamount approximately 60 km SSW of the southernmost point of Guam, with a value exceeding 10,200 m. The base of this seamount is located in the Mariana Trench, which measures the greatest dry submission on Earth with the same value. Outside the vicinity of the Mariana Trench, Mauna Kea in Hawaii also has a significant dry dominance of just over 9300 m, measured from its base on the ocean floor.

Table 3: Datumless point measures (unit: meters) at various summits on Earth.

Mountain	Mountain Range	dom	sub	jut	rut	Elev	Prom
Mt. Washington	Appalachians	1751	0	381	0	1917	1874
Pikes Peak	Rocky Mountains	2575	0	517	0	4301	1680
Grand Teton	Rocky Mountains	2421	0	1125	0	4197	1990
Half Dome	Sierra Nevada	2235	1252	1093	68	2694	414
Mt. Whitney	Sierra Nevada	3955	0	757	0	4419	3072
Mt. Rainier	Cascade Range	4193	0	1266	0	4392	4037
Mt. Robson	Rocky Mountains	3157	0	1907	0	3959	2819
Denali	Alaska Range	5765	0	2101	0	6190	6140
Aconcagua	Andes	6014	0	1832	0	6962	6962
Mt. Fitz Roy	Andes	3200	0	1776	0	3405	1951
Kilimanjaro	East African Rift	5067	0	1367	0	5895	5885
Table Mountain	Cape Fold Belt	1085	473	465	3.0	1085	1055
Matterhorn	Alps	3952	233	1364	3.8	4476	1038
Mont Blanc	Alps	4364	0	1730	0	4810	4697
Mt. Elbrus	Caucasus Mountains	4925	0	1106	0	5642	4741
Kirkjufell	Snæfellsnes Peninsula	472	527	259	52	469	449
Mt. Everest	Himalaya	8081	0	2109	0	8849	8849
Nanga Parbat	Himalaya	7043	0	3166	0	8125	4608
K2	Karakoram	5831	0	2542	0	8614	4020
Mt. Fuji	NE Japan Arc	3731	0	1062	0	3776	3776
Puncak Jaya	Sudirman Range	4842	0	1303	0	4884	4884
Mt. Kosciuszko	Snowy Mountains	1911	0	369	0	2228	2228
Vinson Massif	Sentinel Range	4584	0	1161	0	4892	4892
Unnamed (Dry)	Mariana Arc	10284	124	1410	1.0	-27	148
Mauna Kea (Dry)	Hawaiian Volcanoes	9333	0	1203	0	4205	9330

Table 4: Datumless point measures (unit: meters) at various non-summit locations on Earth.

Location	dom	sub	jut	rut	Elev
San Francisco	16	991	0.2	25	17
Denver	60	2476	0.3	105	1627
Mt. Sunflower	142	46	1.3	0.1	1231
Mirror Lake	808	2682	19	1034	1263
Whitney Portal	2123	1862	134	680	2552
Crater Lake	1281	862	32	89	1882
Mather Point	1462	1060	710	13	2170
Addis Ababa	527	1075	6.0	64	2293
Kathmandu	935	6147	26	492	1307
Everest Base Camp	4558	3477	309	1510	5364
Lhasa	31	2728	0.6	287	3656
Challenger Deep (Dry)	0	8892	0	1274	-10923

5.2.2 Moon, Mars, and Vesta

The datumless measures are particularly handy on planets without a sea level, as they directly describe relief relative to local terrain (as opposed to elevation, whose values need to be compared with other elevation values for this purpose). Generally, smaller planets tend to feature greater relief as quantified by the datumless measures. This is likely due to the lower gravitational pull allowing higher mountains to form at isostatic equilibrium [28].

The Moon is significantly more rugged than the Earth when it comes to averages. Lunar terrain is fairly neutrally skewed, as asteroid impacts tend to generate a similar degree of protruding and recessed features. The far side of the moon facing away from Earth is more rugged than the near side. The point with the highest elevation, known as the Selenian Summit, measures a dominance of slightly over 8300 m and a jut of slightly over 1100 m. However, some places with a lower elevation feature even greater relief, with range exceeding 9000 m and fluctuation exceeding 2000 m in a few locations on the far side. The greatest measured dominance and jut values take place at an unnamed summit approximately 200 km northwest of the Lippmann Crater, with dominance exceeding 10,000 m and jut exceeding 2600 m. The near side of the Moon is less rugged than the far side, containing several maria—large, flat impact basins whose central locations typically measure a fluctuation below 10 m. The famous Montes Apenninus mountain range near the Apollo 15 landing site measures dominance values above 5000 m and jut values above 2000 m in places, with the highest dominance measured atop Mons Huygens.

Mars is a land of topographic extremes, with superlative point measures exceeding those of the Moon. The shield volcano Olympus Mons measures the highest dominance on the planet, with a summit dominance of just over 14,100 m. Despite this, Olympus Mons rises very gradually, as demonstrated by the low domangle of its summit. In fact, the summit is below the horizontal plane of some points at the bottom of the volcano's lower cliffs. Certain points on the slopes of Olympus Mons measure a range exceeding the summit's dominance by a fair amount, with occasional values over 17,000 m. Mars is also home to the giant Valles Marineris canyon, with several times the relief of the Grand Canyon, measuring over 10,000 m of submission or over 3000 m of rut in parts of its rim. Yet another notable feature on Mars is the Hellas Planitia impact basin. Locations near the rim of the basin can measure a range of over 5500 m and a fluctuation of over 1000 m, but points in its central portions typically measure a low fluctuation below 10 m, indicative of flat surroundings. The northern hemisphere of Mars contains large swaths of plains that also consistently measure fluctuation values below 10 m.

Of all the planetary bodies mentioned in this paper, Vesta is by far the most rugged. The most salient feature on Vesta is Rheasilvia, an impact crater with a central peak near the south pole. The central peak measures a dominance of over 16,000 m, even greater than that of Olympus Mons. The rim measures even higher dominance values upwards of 18,000 meters. Fluctuation can exceed 19,000 m in some parts of the Rheasilvia region. The equatorial and northern regions of Vesta are comparatively less rugged, but still very much so. The Divalia Fossa canyon near the equator has less relief than Valles Marineris on Mars, but still significantly more relief than the Grand Canyon. Overall, Vesta is extremely rugged, with even the flattest locations measuring thousands of meters of range and hundreds of meters of fluctuation.

Table 5: Datumless point measures (units: meters) on Moon, Mars, and Vesta.

Planet	Location	dom	sub	jut	rut
Moon	Apollo 11 Landing Site	372.8	237.3	6.8	3.1
	Apollo 15 Landing Site	773	3957	23	780
	Mons Hadley	4726	0	1953	0
	Mons Huygens	5151	0	1570	0
	Selenian Summit	8352	0	1147	0
	Unnamed Summit, ~200 km NW of Lippmann	10806	0	2600	0
	Mare Imbrium, Central	79	7	0.7	0.01
Mars	Olympus Mons, Summit	14175	0	947	0
	Olympus Mons, NW Clifftop	13361	345	2836	0.5
	Valles Marineris, Coprates Chasma, Floor	0	10379	0	1922
	Valles Marineris, Candor Chasma, Rim	8048	2310	3562	67
	Hellas Planitia, Central	75	414	1.1	4.5
	Curiosity Landing Site	53	4808	0.4	761
	Mt. Sharp	4904	0	1507	0
Vesta	Rheasilvia, Central Peak	16321	0	3060	0
	Rheasilvia, Floor	0	16916	0	4108
	Rheasilvia, Rim	18920	287	6492	11
	Divalia Fossa, Floor	0	4332	0	1235
	Feralia Planitia, Floor	611	8647	114	2133

6 Future Work

Future work on the concepts in this paper will likely focus on the following areas:

- Computing the datumless point measures at more places with greater accuracy.
- Developing an algorithm to compute the datumless surface measures.
- Creating more datumless point measures (discussed below).

6.1 More Datumless Point Measures

The datumless point measures in this paper describe relief in terms of maximums in a point's surroundings. While convenient, there are many other ways of describing relief. Currently under development is a set of datumless point measures that describe the relief of a point relative to the direction of least relief. An example would be the rise of Mt. Everest above the Tibetan Plateau, rather than above the Indo-Gangetic Plain, as measured by dominance. Also under development is a set of datumless point measures that describe the average relief of a point relative to its surroundings, rather than the maximum relief. Additional work in progress includes a datumless measure of the independence of a peak, similar to prominence, but designed to be more perceptually accurate and not relying on a datum.

7 Acknowledgements

Thank you to everyone who helped make this paper a reality.

Thank you to Tony Wang for revising the mathematical notation to make it clear and concise. You are truly a genius and a wonderful mentor, and it means a lot for this paper to be read by you.

Thank you to Mr. Behrooz Shahrivini for teaching me so many of the mathematical concepts used in this paper. It brings me joy and fulfillment to apply what I learned in your class to “spicy problems,” as you would often say.

Thank you to the Yale Undergraduate Research Association for providing the opportunity to present several key ideas in this paper at the Yale Undergraduate Research Symposium.

Thank you to Dr. Mark Brandon for teaching me what a geoid is. I once thought I could write this entire paper without knowing such fundamentals—you gladly proved me wrong.

Thank you to Mrs. Pamela Meuser for kindling my interest in STEM subjects when I was in elementary school. You have unknowingly set the trajectory for so many of my current goals and undertakings.

Thank you to all my friends for flying together with me during this journey. I must apologize for my excessive rants about mountains during this weird phase of my life.

Last but not least, thank you to my parents, Helen Kang and Vince Xu, for supporting me through all the ups and downs of the complex topography of life.

8 References

- [1] N. Balasubramania, “Definition and Realization of a Global Vertical Datum,” Ph.D. dissertation, 1994. [Online]. Available: <https://www.proquest.com/dissertations-theses/definition-realization-global-vertical-datum/docview/304101375/se-2>.
- [2] M. A. Wieczorek, “10.05 - Gravity and Topography of the Terrestrial Planets,” in *Treatise on Geophysics*, Elsevier, 2007, pp. 165–206. DOI: <https://doi.org/10.1016/B978-044452748-6.00156-5>.
- [3] E. Earl and D. Metzler, “Cloud-Capped Towers: Capturing Terrain Characteristics Using Topographic Functionals,” *Quaestiones Geographicae*, vol. 34, pp. 7–23, Dec. 2015. DOI: [10.1515/quageo-2015-0033](https://doi.org/10.1515/quageo-2015-0033).
- [4] E. Gadelmawla, M. Koura, T. Maksoud, I. Elewa, and H. Soliman, “Roughness Parameters,” *Journal of Materials Processing Technology*, vol. 123, pp. 133–145, Apr. 2002. DOI: [10.1016/S0924-0136\(02\)00060-2](https://doi.org/10.1016/S0924-0136(02)00060-2).
- [5] J. D. Hunter, “Matplotlib: A 2D Graphics Environment,” *Computing in Science & Engineering*, vol. 9, no. 3, pp. 90–95, 2007. DOI: [10.1109/MCSE.2007.55](https://doi.org/10.1109/MCSE.2007.55).
- [6] K. Thyng, C. Greene, R. Hetland, H. Zimmerle, and S. DiMarco, “True Colors of Oceanography: Guidelines for Effective and Accurate Colormap Selection,” *Oceanography*, vol. 29, no. 3, 2016. DOI: [10.5670/oceanog.2016.66](https://doi.org/10.5670/oceanog.2016.66).

- [7] N. Gorelick, M. Hancher, M. Dixon, S. Ilyushchenko, D. Thau, and R. Moore, “Google Earth Engine: Planetary-Scale Geospatial Analysis for Everyone,” *Remote Sensing of Environment*, 2017. DOI: 10.1016/j.rse.2017.06.031.
- [8] G. Alberti, “Geometric Measure Theory,” *Encyclopedia of Mathematical Physics*, vol. 2, pp. 520–527, Dec. 2006. DOI: 10.1016/B0-12-512666-2/00486-7.
- [9] T. Tadono, H. Ishida, F. Oda, S. Naito, K. Minakawa, and H. Iwamoto, “Precise Global DEM Generation by ALOS PRISM,” *ISPRS Annals of Photogrammetry, Remote Sensing and Spatial Information Sciences*, vol. II-4, pp. 71–76, Mar. 2014. DOI: 10.5194/isprs-annals-II-4-71-2014.
- [10] J. Takaku, T. Tadono, and K. Tsutsui, “Generation of High Resolution Global DSM from ALOS PRISM,” *ISPRS - International Archives of the Photogrammetry, Remote Sensing and Spatial Information Sciences*, vol. XL-4, pp. 243–248, Mar. 2014. DOI: 10.5194/isprs-archives-XL-4-243-2014.
- [11] J. Takaku, T. Tadono, K. Tsutsui, and M. Ichikawa, “Validation of ‘AW3D’ Global DSM Generated from ALOS PRISM,” *ISPRS Annals of Photogrammetry, Remote Sensing and Spatial Information Sciences*, vol. III-4, pp. 25–31, Jun. 2016. DOI: 10.5194/isprs-annals-III-4-25-2016.
- [12] T. Tadono, H. Nagai, H. Ishida, F. Oda, S. Naito, K. Minakawa, and H. Iwamoto, “Generation of the 30 M-Mesh Global Digital Surface Model by ALOS Prism,” *ISPRS - International Archives of the Photogrammetry, Remote Sensing and Spatial Information Sciences*, vol. XLI-B4, pp. 157–162, Jun. 2016. DOI: 10.5194/isprs-archives-XLI-B4-157-2016.
- [13] P. Weatherall, K. M. Marks, M. Jakobsson, T. Schmitt, S. Tani, J. E. Arndt, M. Rovere, D. Chayes, V. Ferrini, and R. Wigley, “A New Digital Bathymetric Model of the World’s Oceans,” *Earth and Space Science*, vol. 2, no. 8, pp. 331–345, Jun. 2015. DOI: 10.1002/2015EA000107.
- [14] F. Lemoine, S. Kenyon, J. Factor, R. Trimmer, N. Pavlis, D. Chinn, C. Cox, S. Klosko, S. Luthcke, M. Torrence, Y. Wang, R. Williamson, E. Pavlis, R. Rapp, and T. Olson, “The Development of the Joint NASA GSFC and the National Imagery and Mapping Agency (NIMA) Geopotential Model EGM96,” Jul. 1998. [Online]. Available: <https://ntrs.nasa.gov/citations/19980218814>.
- [15] Agisoft, *EGM96 15’ Geoid Model*, 2022. [Online]. Available: <https://www.agisoft.com/downloads/geoids/>.
- [16] LOLA Science Team, *Moon LRO LOLA DEM 118m v1*, Planetary Data System, Mar. 2014. [Online]. Available: https://astrogeology.usgs.gov/search/map/Mars/Topography/HRSC_MOLA_Blend/Mars_HRSC_MOLA_BlendDEM_Global_200mp_v2.
- [17] USGS Astrogeology Science Center, *Mars MGS MOLA - MEX HRSC Blended DEM Global 200m v2*, Planetary Data System, Jan. 2018. [Online]. Available: https://astrogeology.usgs.gov/search/map/Mars/Topography/HRSC_MOLA_Blend/Mars_HRSC_MOLA_BlendDEM_Global_200mp_v2.

- [18] F. G. Lemoine, D. E. Smith, D. D. Rowlands, M. T. Zuber, G. A. Neumann, D. S. Chinn, and D. E. Pavlis, “An Improved Solution of the Gravity Field of Mars (GMM-2B) from Mars Global Surveyor,” *Journal of Geophysical Research: Planets*, vol. 106, no. E10, pp. 23 359–23 376, 2001. DOI: 10.1029/2000JE001426.
- [19] NASA/JPL-Caltech/UCLA/MPS/DLR/IDA, *Vesta Dawn FC HAMO Global DTM 93m v1*, Planetary Data System, Dawn Team, Dec. 2013. [Online]. Available: https://astrogeology.usgs.gov/search/map/Vesta/Dawn/DLR/HAMO/Vesta_Dawn_HAMO_DTM_DLR_Global_48ppd.
- [20] R. A. Beyer, O. Alexandrov, and S. McMichael, “The Ames Stereo Pipeline: NASA’s Open Source Software for Deriving and Processing Terrain Data,” *Earth and Space Science*, vol. 5, 2018. DOI: 10.1029/2018EA000409.
- [21] B. Hofmann-Wellenhof, H. Lichtenegger, and J. Collins, *Global Positioning System: Theory and Practice*. Feb. 2001. DOI: 10.1007/978-3-7091-6199-9.
- [22] C. Russell, C. Raymond, A. Coradini, H. McSween, M. Zuber, A. Nathues, M. C. De Sanctis, R. Jaumann, A. Konopliv, F. Preusker, S. Asmar, R. Park, R. Gaskell, H. Keller, S. Mottola, T. Roatsch, J. Scully, D. Smith, P. Tricarico, and T. Titus, “Dawn at Vesta: Testing the Protoplanetary Paradigm,” *Science (New York, N.Y.)*, vol. 336, pp. 684–6, May 2012. DOI: 10.1126/science.1219381.
- [23] Google. (2022). “Google Maps,” [Online]. Available: <https://maps.google.com/>.
- [24] Peakbagger.com. (2022), [Online]. Available: <https://peakbagger.com/>.
- [25] A. Helman, *The Finest Peaks: Prominence and Other Mountain Measures*. Trafford Publishing, 2005.
- [26] J. Robl, S. Hergarten, and G. Prasicek, “Glacial Erosion Promotes High Mountains on Thin Crust,” *Earth and Planetary Science Letters*, vol. 538, 2020. DOI: 10.1016/j.epsl.2020.116196.
- [27] C. Ammann, B. Jenny, K. Kammer, and B. Messerli, “Late Quaternary Glacier Response to Humidity Changes in the Arid Andes of Chile (18–29° S),” *Palaeogeography, Palaeoclimatology, Palaeoecology*, vol. 172, no. 3, pp. 313–326, 2001. DOI: 10.1016/S0031-0182(01)00306-6.
- [28] A. B. Watts, *Isostasy and Flexure of the Lithosphere*. Jan. 2001, vol. 458, p. 458.